Dynamic Properties of Isotropic DMPC/DHPC Bicelles: Insights from Solution NMR and MD Simulations

Bon Leif Dominguez Amalla[a], Hiroyuki Kumeta[b], Satoshi Nagao[c], and Koichiro Ishimori[a,d]

[a]Graduate School of Chemical Sciences and Engineering, Hokkaido University, N13, W8, Sapporo 060-8628, Japan

[b]Frontier Research Center for Advanced Material and Life Science, Graduate School of Life Science and Faculty of Advanced Life Science, Hokkaido University, N21, W11, Sapporo 001-0021, Japan

[c]Japan Synchrotron Radiation Research Institute, 1-1-1 Kouto, Sayo-cho, Sayo-gun, Hyogo 679-5198, Japan

[d]Department of Chemistry, Faculty of Science, Hokkaido University, N8, W5, Sapporo 060-0810, Japan

Corresponding Author: Koichiro Ishimori (koichiro@sci.hokudai.ac.jp)

ABSTRACT

Bicelles, an artificial disk-shaped lipid bilayer, are commonly used for the structural and functional characterization of membrane-bound proteins in an environment similar to that in intracellular membranes. Because the dynamics of the lipids that constitute bicelles exert a significant impact on the structure and function of the inserted proteins, we investigated the mobility of lipid molecules in bicelles composed of DMPC (14:0 PC) and DHPC (06:0 PC) using solution NMR and MD calculations. ^{13}C R_1 relaxation experiments for the acyl groups demonstrated that increasing bicelle sizes limit the rotational diffusion of acyl chain H–C bonds in DMPC. Such a limited local motion around H–C bonds was also predicted in the MD simulations of DMPC bilayers with decreased area per lipid, indicating that the limited mobility of the hydrophobic core in larger bicelles is due to the tighter lipid packing. The downfield shifts of the ^{13}C NMR signals of the acyl groups supported the restricted mobility, corresponding to the conformational changes of the acyl chains from the flexible *gauche* rotamers to the less mobile *trans* rotamers with increase in bicelle size. These data suggest that larger bicelles pack lipids more densely, leading to increased *trans* conformation of the acyl chains and, consequently, less lipid motility, which can dynamically modulate the structure and function of membrane-bound proteins inserted into the bicelles.

KEYWORDS*:* DMPC; DHPC; bicelles; NMR; lipid dynamics; MD simulation

1. Introduction

Intracellular lipid bilayers not only delimit the intracellular space and anchor membrane-bound proteins in their appropriate locations but also regulate the structure and function of membrane-bound proteins through specific and nonspecific interactions based on their physical properties such as hydrophobicity, charge, fluidity, and mobility [1]. The contribution of such interactions to various biological processes, including metabolism, trafficking, signaling, and transmembrane transport, has been proposed [2-5], and these interactions are obviously essential for maintaining life. There are extensive data on the effects of hydrophobicity inside the membrane and charge of the membrane surface on the structure and function of protein in lipid bilayers; however, there is limited knowledge on how the dynamic properties of lipid bilayers, such as fluidity and mobility, affect the structure and function of protein, which is due to the experimental difficulty of directly tracking these dynamic properties [6].

Although the effects of the dynamic properties of lipid bilayers on the structure and function of membrane-bound proteins are not completely understood, in recent years, there has been increasing research on the structural and functional characterization of membrane proteins by reconstituting proteins into artificial lipid bilayers [7]. Several conventional studies on the structure and function of membrane proteins have used membrane-bound proteins solubilized with detergents. However, in such cases, the interactions of the protein with the detergent micelles were assumed to be extremely different from its interactions with the lipid bilayer in cells, and the structural and functional characterization of membrane-bound proteins solubilized by detergent micelles may not accurately reflect the structure and function of membrane-bound proteins in cells. Although homogeneous artificial lipid membranes cannot perfectly reproduce natural lipid bilayers in terms of the diversity of lipid molecules, the presence of bilayer sides, and the curvature of the bilayer, the macroscopic properties as a lipid bilayer are assumed to have a significant effect on membrane-bound proteins, artificial lipid bilayers such as bicelles, nanodiscs, and liposomes are used for the structural and functional characterization of membrane-bound proteins [8-10].

Among artificial lipid bilayers, bicelles, composed of two types of lipids, one with long acyl chains and the other with short chains, have the advantage that no scaffold proteins altering the membrane fluidity and lipid mobility are used: however, they are structurally less stable than other lipid bilayer models and are stable only under specific conditions. Nevertheless, their size, unlike liposomes, can be maintained within the range where detailed spectroscopic measurements can be applied [10]. However, detailed analyses of the dynamic properties of lipids—such as their mobility, flexibility, and intermolecular interactions—within bicelles have not yet been reported. Furthermore, the factors that determine their dynamic property also need to be clarified. In particular, unlike natural lipid bilayers, bicelles have a disk-like structure with a short lipid rim region surrounding their lipid bilayer core. Unfortunately, there are also no data on the optimal bicelle size as a model for a natural lipid bilayer because of the limited information on the dependence of the dynamic properties of the lipids on the size

of the bicelle. Previous ^{1}H NMR translational diffusion measurements of small DMPC/DHPC bicelles with different *q* ([DMPC]/[DHPC]) ratios (0.25 and 0.5) have revealed that a smaller diffusion coefficient was observed for bicelles with higher *q* ratios, indicating that the diffusion of lipid molecules is suppressed in larger bicelles [11]. Conversely, the order parameters of lipids estimated from EPR spectra obtained with spin-labeled lipids are almost independent of the size of the bicelle, suggesting that restriction of the local motion in the lipids remains unchanged with the increase in the size of the bicelle [11]. In larger bicelles as used for lipid bilayer models to embed membrane proteins, however, the dynamics of the lipids, particularly variations in conformations of the lipid headgroups and acyl chain interacting with embedded proteins, remain unclear.

In this study, bicelles of different sizes were prepared, and based on their solution ^{13}C NMR and MD simulations, the dependence of the conformation and local mobility of lipid acyl chains on the size of the bicelles was investigated. The NMR measurements provide information on the local mobility of lipid molecules in the millisecond-to-second range that affects the overall motion of membrane-bound proteins, as well as information on the conformation of lipid molecules. Combined with the correlation between the density of lipid molecules in the lipid bilayer and the rotational correlation time by MD simulation, the size dependence of the dynamic properties of the bicelles is discussed. The dynamic properties of bicelles obtained in this study will provide fundamental knowledge to optimize the size of bicelles for the reconstituting membrane-bound proteins and for regulating the structure and function of membrane-bound proteins using lipid–protein interactions in the bicelles.

2. Materials and methods

2.1. Sample preparation

Lipids (DMPC and DHPC) in powder form were obtained from Avanti Polar Lipids, Inc. Bicelle solutions are prepared similarly as reported previously [12,13] with some modifications. DMPC/DHPC lipid solutions were prepared by first dissolving DHPC powder in 50 mM sodium phosphate buffer with pH 6.8 (NaPi buffer) in a dry environment so that its concentration is >100 mM, making concentrated DHPC micelle solutions. Then, appropriate amounts of DMPC powder were added to the micelle solution to achieve the desired *q* ratios between 0.5 and 1.2. Finally, the total lipid concentrations ([PC]) were adjusted to 100 mM by diluting with NaPi buffer. The lipid aggregates were homogenized using four freeze–thaw cycles: the lipid solutions were flash-frozen with liquid nitrogen and thawed in a 45°C-water bath for 3 min. NMR samples were prepared by further addition of D_2O for frequency locking. The final concentration of D_2O in the samples was 5% (v/v). Finally, the solutions were further homogenized and mixed by gentle ultrasonication for 10 min at 25°C. In line with previous reports [12,13], measurements were conducted under conditions that ensured the bicelles were isotropic and stable. To confirm the isotropic property of the bicelles, we measured the ^{31}P NMR spectra as previously reported (Fig. 1). Fig. 1A displays the presence of phospholipids near 0 ppm, indicating isotropically

tumbling species. The absence of signals between -10 and -20 ppm suggests that the bicelles in the samples are isotropic [14]. The ^{1}H decoupled ^{31}P spectra (Figs. 1B and 1C) can be simulated by the sum of two Lorentzian distribution functions, fitting well with relative RMSD values of 0.0023 and 0.0019, respectively, which implies that the lipid phases are homogeneous, particularly for DMPC [12,13]. The line broadening observed for both DHPC and DMPC with increasing q is likely attributed to the slower rotation of the bicelles, as evidenced by the faster R_2 relaxation of the headgroup methyl protons, rather than lipid phase heterogeneity.

2.2. NMR spectroscopy

Spectra were obtained using a Bruker Avance III HD spectrometer equipped with a triple resonance 5-mm TXI probe operating at a Larmor frequency of 600 MHz for ^{1}H. ^{13}C spectra were obtained at the natural abundance of the isotope. Unless otherwise specified, NMR samples were set into 5-mm Shigemi sample tubes and all spectra were obtained at 25°C. Samples were allowed to equilibrate at the measurement temperatures and the magnetic field for at least 5 min before frequency locking. All spectra were processed using Topspin 3.2/3.6.

One-dimensional ^{1}H spectra were obtained using a 90° pulse-acquire sequence with solvent peaks suppressed by presaturation. The ^{1}H-decoupled DEPT-45 pulse sequence was used to obtain one-dimensional ^{13}C spectra of nuclei with attached protons, *i.e.*, those in the acyl chains and headgroup. Resonance assignments were performed using ^{1}H-^{13}C HSQC and HSQC-TOCSY experiments with an echo/anti-echo acquisition type. Parameters for these experiments were available in the Topspin 3.2 distribution.

^{1}H R_2 experiments were conducted using a Carr-Purcell-Meiboom-Gill spin echo pulse train with presaturation. The pulse train has the structure $(t\text{-}180°\text{-}t\text{-}90°\text{-}t\text{-}180°\text{-}t)_n$-acquire where the spin echo delay t is set to 2.5 ms and 10 counters n are selected between 2 and 600. The perfect echo structure was used to obtain undistorted line shapes from undesired J-modulations in acyl chain signals. The inversion-recovery pulse sequence with a ^{1}H-decoupling pulse during acquisition was used for the ^{13}C R_1 experiments. A total of 12 relaxation delays from 0.05 s to 10 s were used.

^{1}H-decoupled ^{31}P NMR spectra were obtained using a Bruker Avance III spectrometer equipped with a 5-mm broadband observe BBO probe, tuned to the Larmor frequency of ^{31}P at 242.9 MHz. A 30° pulse-acquire pulse sequence was employed with a pulse length of 13 μs, utilizing a WALTZ16 proton decoupling scheme during signal acquisition (0.341 s) and the relaxation delay of 2.0 s. These experiments were conducted in the Topspin 3 software using the P31CPD protocol.

2.3. Spectrum analysis

The NMR spectra processed using Topspin 3.2/3.6 were analyzed using in-house routines written in Julia v1.10. The DEPT-45 spectra were processed with an exponential line broadening of 1 Hz before Fourier transform. Numerical integrations were performed using the trapezoidal quadrature rule. The resonances used for the spectrum analyses along with their typical chemical shift ranges are summarized in Table 1. The integrated intensities of acyl chain methyl ^{1}H resonances for CH_3(DMPC) and CH_3(DHPC) were used to estimate their relative ratio in the bicelle solutions and the q ratio (Eq. 1). Chemical shift perturbations of acyl chain ^{13}C resonances ($C_{4\text{-}11}$, C_{12}, and C_{13}) were described as changes in first moments μ_1' (Eq. 2). The standard errors of μ_1' are estimated by including contributions from noise in the intensity values after processing. The R_2 relaxation rate constants for the acyl chain $C\underline{H}_3$ and choline headgroup methyl protons and the R_1 relaxation rate constants for DMPC acyl chain, $C_{4\text{-}11}$, C_{12}, and C_{13}, were estimated by fitting the integrated intensities against the delays before the acquisition using a single exponential decay model (Eq. 3) and by nonlinear fitting of the integrated intensities against the relaxation delays using Eq. 4, respectively.

$$q = \frac{\int_{\mathrm{CH_3(DMPC)}} I(\delta)\, d\delta}{\int_{\mathrm{CH_3(DHPC)}} I(\delta)\, d\delta} \tag{1}$$

$$\mu_1'(\mathrm{C}_n) = \frac{\int_{\mathrm{C}_n} \delta \cdot I(\delta)\, d\delta}{\int_{\mathrm{C}_n} I(\delta)\, d\delta} \tag{2}$$

$$I(\tau; H_n) \equiv \int_{\mathrm{C}_n} I(\delta)\, d\delta = A \cdot \exp(-R_2\tau) \tag{3}$$

$$I(\tau; \mathrm{C}_n) \equiv \int_{\mathrm{C}_n} I(\delta)\, d\delta = A_1 \cdot [1 - A_2 \exp(-R_1\tau)] \tag{4}$$

Hypothesis tests for the equality of relaxation rate constants were conducted using two-tailed *t*-tests with a significance level α of 0.05. The number of degrees of freedom for the R_2 and R_1 tests are 8 and 10, respectively.

The ^{1}H-decoupled ^{31}P spectra were processed with an exponential line broadening of 1 Hz prior to Fourier transform. Nonlinear least squares fitting of the spectra, as sums of two Lorentzian distributions corresponding to DHPC and DMPC, was performed using in-house routines written in Julia v1.10. The residuals after fitting were used to confirm the homogeneity of the DMPC lipid phases within the range of q values explored in the experiments.

2.4. Molecular dynamics simulations of pure DMPC bilayers

Molecular dynamics (MD) simulations of fluid DMPC bilayers were conducted using the GROMACS v2023.3 MD engine [15] with the Slipids 2020 force field [16,17]. The simulation box containeding 128 lipids with 30 TIP3 water molecules per lipid for sufficient hydration and equilibrated for 500 ns at 303 K were obtained from the official Slipids web site (http://www.fos.su.se/~sasha/SLipids/Downloads.html). As recommended for the force field, the electrostatic interactions in the periodic simulation box were calculated using the Particle-Mesh-Ewald (PME) method [16,17] with 0.12 nm Fourier spacing. The Lennard-Jones interactions were calculated with a cut-off radius of 1.4 nm [16,17]. Distance constraints on the lipid and TIP3 bonds were solved using the LINCS algorithm as implemented in the MD engine. These MD parameters are included in the example MD parameter input files in the official web site.

The DMPC area per lipid (APL) in each simulation was varied by surface tension coupling implemented in the MD engine. Eight reference values for the surface tension were selected between 120 bar·nm and 840 bar·nm. The temperature (303 K) and surface tensions in the equilibration and sampling simulations were maintained using the velocity and stochastic cell rescaling algorithms implemented as the *v*-rescale thermostat and *c*-rescale barostat in the MD engine, respectively. Both equilibration and sampling simulations were 100-ns long, resulting in 200-ns long trajectories.

Trajectories were analyzed using in-house routines written in Julia v1.10. For each simulation, the average APL or $\langle A \rangle_t$ was calculated as the area of the simulation box averaged over each simulation snapshot, *i.e.*, over time, divided by the number of lipids in each leaflet $n_{lip}/2 = 64$, according to Eq. 5. The simulation box dimensions $L_{x,y}$ were obtained using the gmx energy utility of the MD engine. We assumed that the equilibrium of the APL is reached when there is minimal drift in its value. The rotational diffusion of the acyl chain H–C bonds was evaluated based on the decay of the time correlation function (τ_{cf}) of their orientations with respect to the membrane normal (z-axis) according to Eq. 6. The tcfs were fitted against single exponential functions (Eq. 7), deriving decay rate constants $1/\tau_c$. Assuming that the decay rate constants vary slowly and continuously with the APL, a simple linear regression was performed to show a relationship between the $1/\tau_c$ rate constants and the APL. The statistical significance of the linear regression model was determined using an *F*-test of overall significance with *dof* = 6 and significance level α of 0.05.

$$\langle A \rangle_t = \frac{2\langle L_x L_y \rangle_t}{n_{lip}} \tag{5}$$

$$C(\tau) = \langle P_2(\cos\theta(t)) \cdot P_2(\cos\theta(t+\tau)) \rangle_t \qquad P_2(\cos\theta) = \frac{1}{2}(3\cos^2\theta - 1) \tag{6}$$

$$C(\tau) = A \cdot \exp\left(-\frac{\tau}{\tau_c}\right) \tag{7}$$

3. Results

3.1. Resonance assignments

DHPC acyl chain signals were assigned by assuming a fast exchange of DHPC between the bicelle and buffer solution [13,18,19], which implies that the observed chemical shifts of DHPC acyl chains ^{13}C are averages of the chemical shifts in the bicelle and solution, weighted by their relative amounts. Therefore, dilution of bicelle solutions causes upfield shifts of the DHPC signals. DEPT-45 spectra of the bicelle solutions with q = 0.5 but different [PC], *viz.*, [PC] = 100 or 50 mM, were obtained (Fig. 2A). Sharp resonances that shifted upfield upon dilution were assigned to DHPC. We suspect that the two peaks comprising each DHPC resonance may have originated from the DHPC *sn*-1 or *sn*-2 chains, but they were not further assigned. Headgroup signals were assigned from the ^{1}H–^{13}C correlation spectra of bicelles with q = 0.5 and [PC] = 100 mM (Fig. 2B). A one-to-one correspondence between headgroup ^{1}H and ^{13}C resonance indicates that the resonances of headgroups of DHPC and DMPC in the bicelle rim and core, respectively, are not separated.

Assignments along the acyl chains were performed with ^{1}H–^{13}C HSQC and HSQC-TOCSY spectra of bicelles with q = 0.5 and q = 1.0 with [PC] = 100 mM, respectively (Fig. 2C). Separating the DHPC acyl chain methyl signals allowed the identification of DMPC acyl chain $C_{12\text{-}14}$ signals. Finally, coupling between DHPC C_2 and C_3 carbons allowed the assignment of DMPC C_3 and the central $C_{4\text{-}11}$ chain by elimination.

To determine the phase of the DMPC lipid bilayer core, the DEPT-45 spectra of bicelles were compared with those of a reference fluid bicelle system at 308 K as a reference (Fig. 2D). The DMPC C_{12} and C_{13} resonances showing two peaks were used as markers. Similar to DHPC resonances, these resonances originated from the *sn*-1 and *sn*-2 acyl chains having different local environments, as reported previously [11]. The presence of peaks apart from these indicates the possible coexistence of bicelles in the gel phase and liquid-crystalline phase [13,20]. The DEPT-45 spectra of bicelle samples with q ratios between 0.5–1.2 exhibited (not shown) no such patterns, indicating that all samples were in the liquid-crystalline phase. Furthermore, given that the range of q ratios employed in this study closely aligns with those utilized by Kot et al. [12,13], the bicelles in this study are also isotropic, meaning they exhibit isotropic tumbling behavior, and are in the liquid-crystalline phase. Although 25°C is near the phase transition temperature (T_m) for DMPC/DHPC bicelles, neither the onset of the phase transition nor the presence of a metastable state has been detected. This observation is consistent with previous reports [12,13].

3.2. Increased bicelle sizes slow down H–C bond rotational diffusion

Previous studies have reported that the size of bicelles depends on q ratios, and [PC] [18,19,21,22]. Two bicelle solutions with different average particle sizes, *viz.*, q = 0.5 and q = 1.0, under [PC] = 100 mM, were prepared. Small angle neutron scattering dilution measurements revealed that between the compositions of q = 0.2 and q = 1.0 and temperatures of T = 10°C and 40°C, bicelle mixtures adopt the idealized disk-shaped morphologies, in which the planar bilayer radius, R, ranged from 21 Å (q = 0.2) to 77 Å (q = 1.0) [21]. The increase in bicelle size by increasing q ratios was confirmed through ^{1}H R_2 relaxation rates. As shown in Table 2, the ^{1}H R_2 relaxation rate for bicelles with q = 0.5 was lower than that for bicelles with q = 1.0, indicating that the size of the bicelles with q = 1.0 was larger than that of the bicelles with q = 0.5 under the same concentration [PC] = 100 mM.

The changes in local moiety motion were observed for the H–C bonds of the acyl and headgroups through ^{13}C R_1 experiments using bicelles with q = 0.5 and q = 1 under [PC] = 100 mM (Fig. 3C, Table 3). Only the R_1 relaxation rate of ^{13}C in the choline methyl group clearly increased with bicelle size, and the R_1 relaxation rates of the $C_{4\text{-}11}$ and C_{13} in the acyl chain also tended to be higher in the larger bicelles. This finding suggests that, as the size of the bicelle increases, the motion of the headgroup H–C bonds of the lipid molecule and the local motion of the H–C bonds of the acyl groups are restricted.

To further explore the restricted local mobility of lipid molecules due to changes in the size of the bicelles, MD simulations were conducted for the rotational diffusion of the H–C bonds in the acyl group of pure DMPC lipids with varying APL. It has been reported that the APL, corresponding to the distribution density of lipid molecules in the lipid bilayer leaflets, exerts significant effects on the motility of lipid molecules [23,24], and previous MD simulations have also indicated that DMPC lipids are more densely packed in larger bicelles [25]. Therefore, rather than conducting molecular dynamics (MD) simulations with bicelles of varying sizes, we directly adjusted the area per lipid (APL) on pure DMPC bilayers. The rotational diffusion rates are expressed as the decay rates of the time correlation function of the angle between the H–C bond and the bilayer normal (z-axis). The correlation decay rates, $1/\tau_c$, for the H–C bond angle in the acyl groups was plotted against the average APL, as depicted in Fig. 4. Although the autocorrelation decay rates of the C_2, C_3, and C_4 carbons were almost constant with varying APL, the correlation decay rates for the C_{11}, C_{12}, and C_{13} carbons increased with APL. Despite the decay rates showing significant variance among the DMPC lipids, tests of overall significance revealed a linear relationship between the average APL and correlation decay rates. The H–C bonds, particularly those closer to the terminal methyl chain, exhibit a more rigid motion under tighter lipid packing. Together with the observed fast R_1 relaxation in larger bicelles, the restricted H–C bond rotation is correlated with tighter lipid packing under lower APL and the increase in bicelle size. This further implies that APL of the DMPC bilayer core is reduced in larger bicelles, corresponding to structural changes in the bilayer, such as acyl chain extension of the DMPC lipids and an increase in bilayer height [3].

3.3. DMPC acyl chain CH_2-CH_2 rotation is affected by bicelle size

In lipid bilayers, changes in the dynamic properties of lipids are often accompanied by the conformational transition of the lipid structure [26]. The extension of lipid acyl chains in increased bicelle sizes can be confirmed through monitoring their conformation. From the R_1 experiments, the one-dimensional spectra for the acyl chains showed downfield shifts of the central $C_{4\text{-}11}$ chains and C_{13} resonances upon the increase in bicelle size (Fig. 3B). These downfield shifts were also observed for the central $C_{4\text{-}11}$ chain signals of DMPC upon bicelle dilution (Fig. 2A). These downfield shifts, however, were not observed for the DMPC acyl chain C_2 or any of the headgroup resonances (Figs. 3A and 3B), indicating the sensitivity of the lipid acyl chain conformations against the size of the bicelle. Similar downfield shifts were reported in a previous solid-state NMR study on DMPC liposomes, corresponding to the conformational changes of the acyl chains from the flexible *gauche* rotamers to the less mobile *trans* rotamers induced by the transition between the gel and the liquid-crystalline phases around the phase transition temperature, T_m [20].

To further investigate the conformational changes of the acyl groups in detail, DEPT-45 measurements were conducted for bicelles with q = 0.78–1.18. Based on the relationship between q ratio and size of bicelles [13], these bicelles have predicted core diameters between about 70 Å and 110 Å. Similar to previous observations, the headgroup and acyl chain C_2 resonances did not shift significantly with increasing q ratios (not shown). Representative spectra of $C_{4\text{-}11}$ and C_{13} resonances are shown in Fig. 5A. The signals from DMPC lipids (Fig. 5A, left) are assumed to be from those in the liquid-crystalline phase due to the similarity of the acyl chain C_{13} signals to the fluid bicelle spectrum (Fig. 2D). All resonances shifted downfield with significant line-broadening as the q ratio is increased. Because the ^{13}C resonances from the *trans* conformer exhibit downfield shifts compared with those from the *gauche* conformer [20], these downfield shifts indicate the increasing population of *trans* conformations involved in the rapid *trans–gauche* conformational exchange on the NMR time scale in larger fluid bicelles. The line-broadening of the NMR signal associated with the downfield shifts (Fig. 5A) corresponds to the faster ^{13}C R_2 relaxation rates with increasing q ratios (Table 2) due to the large molecular weight of larger bicelles. The first moments (Eq. 2) of $C_{4\text{-}11}$ and C_{13} resonances were plotted against q ratios (Fig. 5B). Least-squares regression models indicate a linear relationship between q (bicelle size) and the first moments. Coefficients of the determination (R^2) demonstrated that the linear relationship with the lipid ratio q could explain at least 85% of the variation in the first moments. This suggests that there is a continuous relationship between the size of fluid bicelles and the amount of *trans* and *gauche* conformers along the acyl chains.

4. Discussion

The present NMR and MD simulation results of this study indicate that in bicelles, the mobility of the acyl chains and headgroups of the lipid molecules is suppressed with an increase in bicelle size, and the conformation of the central C_4–C_{11} and C_{13} fragments of the DMPC acyl chain transitions from the mobile *gauche* form to the less mobile *trans* configuration. Such conformational transition was also encountered for the main phase transition from the liquid-crystalline, fluid phase to the gel phase in DMPC liposomes [20] at around 300 K. The ^{13}C resonances from the acyl chains C_3, C_4-C_{11}, and C_{13} in the lipid gel phase at lower temperatures demonstrated downfield chemical shifts, compared to those in the fluid phase at higher temperatures [20]. Such downfield shifts suggest that the acyl chains are fully extended and oriented nearly perpendicular to the plane of the lipid bilayer due to the highly restricted intra- and intermolecular motions. This restriction leads to both short- and long-range ordering within the gelled lipid bilayer, resulting in a highly impermeable structure. Conversely, in the liquid crystalline phase, the acyl chains exhibit increased mobility, which leads to an increase in the effective cross-sectional APL molecule and a concomitant decrease in the bilayer thickness [20].

Similarly, in the case of bicelles, as their size increases both due to dilution and an increase in q, the population of the *gauche* conformer decreases, and the increase in the *trans* conformer implies that the mobility of the lipid molecules decreases with the increase in bicelle size. Similar to the finding that the decrease in the mobility of lipid molecules associated with the transition from the gel phase to the liquid-crystalline phase in DMPC causes a reduction in the effective cross-sectional APL, in the present study, the MD simulation for lipids in bicelles also demonstrated that a decrease in the local mobility of lipid molecules corresponds to the reduction of APL. These findings suggest that with an increase in the size of bicelles, the lipid molecules become more densely packed, and the conformation of the acyl groups transitions to the *trans* conformer from the *gauche* conformer, which indicates the limited mobility of lipid molecules.

Such suppressed mobility of lipids in larger bicelles was also suggested by the diffusion coefficients estimated by ^1H NMR [11]. Bicelles with $q = 0.5$ exhibited a slower diffusion ($D = 2.7 \times 10^{-11}$ m^2s^{-1}) than bicelles with $q = 0.25$ ($D = 7.3 \times 10^{-11}$ m^2s^{-1}) [11]. Although DMPC dissociated from the bicelles significantly contributed to the small diffusion coefficient [11], the slow diffusion of DMPC in large bicelles correlates with the suppressed local mobility of lipid molecules. Conversely, the order parameters calculated from the EPR spectra of the spin-labeled lipids were almost independent of the q ratio, indicating that the motion of the spin-labeled moiety of lipids was insensitive to the size of the bicelles. Interestingly, the order parameters for the headgroup and C_{12} position were in the range of 0.03–0.08, and such low order parameters suggest that the motion around the headgroup and C_{12} of the acyl chains is unrestricted despite the larger size of bicelles [11]. Although such unrestricted rotation and the suppressed mobility of lipid molecules in bicelles demonstrated in this study may contradict each other, the order parameter reflects rotation in the picosecond or nanosecond range of the spin

labeled moiety. In contrast, the relaxation measurement reflects processes in the hundreds of millisecond range, which is in a different time domain for the motion [27].

Although the R_1 relaxation measurements suggest suppression of the local mobility of the acyl group, the changes in R_1 relaxation rates for the central C_4-C_{11} chains and C_{13} signals were not prominent. Despite small changes in the local mobility of the acyl group, the fast R_1 relaxation for the headgroup and conformational changes of the acyl group from the *gauche* conformer to the *trans* conformer were evident (Fig. 5) and the rotational correlation times calculated from simulations also demonstrated a similar trend (Fig. 4). The relatively small changes in the acyl chain R_1 relaxation rates can be attributed to the low signal-to-noise ratio of the signals, especially when compared to the sharp and intense signals of the headgroup methyl group. The subtle but significant changes in lipid mobility are a result of the larger bicelle sizes and the consequent tighter lipid packing.

Considering that the decreased APL in bicelles with a larger q ratio implies the more densely packed lipid molecules in larger bicelles, the tight packing in larger bicelles would suppress the mobility of the headgroup of the lipids and promote the transition from the *gauche* conformer to the *trans* conformer. This conformational transition is an exothermic process [20]. Some of the energy released from the transition would be used to maintain mobility around the H–C bonds of the acyl groups, causing in a smaller decrease in their mobility. Conversely, the lack of such structural changes for the headgroup would significantly suppress its mobility by the dense packing of the lipids in larger bicelles.

Despite the lack of experimental evidence for the origin of the changes in the dynamic properties of lipid molecules depending on the size of the bicelle, it can be assumed that the presence of the rim region in the bicelle exerts significant effects on the dynamic properties of the lipid molecules constituting the bicelle. In the rim region of the bicelle, lipids with short acyl groups form a micelle-like structure instead of a lipid bilayer structure. A previous MD simulation [25] indicated that bicelles with $q = 0.5$, *i.e.*, small bicelles, are more micelle-like than expected by the ideal bicelle model [28], where the DMPC lipids might form a regular bilayer. An interface would be formed between the micelle-like bicelle rim and the lipid bilayer core, where the packing of lipids is not as tight as in other components of the bicelle, and the interface probably has large structural fluctuations. Therefore, the structural fluctuations at the interface between these structures will also enhance the mobility of the lipid molecules in the lipid bilayer near the interface. In other words, in small bicelles, the interface with large structural fluctuations strongly affects the mobility of lipid molecules in the lipid bilayer. However, in large bicelles, the effect is relatively small because of the larger number of lipid molecules away from the interface, and the mobility of lipid molecules would be reduced due to their more densely packed structure in the core region of bicelles. This observation aligns with the conclusion from the previous report [11] that the detergents surrounding the bicelle core disrupt the lipid packing. Moreover, this disturbance is dependent on the extent of lipid exposure at the bicelle rim.

3. Conclusion

The NMR experiments and the MD simulation demonstrated that increasing the sizes of isotropic bicelles results in more densely packed lipids, suppressed local motion of lipid molecules, and conformational transition of the *gauche* conformer to the *trans* conformer. This conformational transition would relieve suppression of the local motion of the acyl groups of lipids, causing to small changes in the R_1 relaxation rate. The dependence of such dynamic properties on the size of bicelles would be attributed to the rim region of bicelles. Therefore, when using bicelles as artificial lipid bilayer models, it will be necessary to consider the dynamic properties of lipids, especially the mobility of the headgroup and the conformation of the acyl chains of the lipid, depending on the size of the bicelle.

Abbreviations: NMR, nuclear magnetic resonance; DMPC, 1,2-dimyristoyl-*sn*-glycero-3-phosphocholine; DHPC, 1,2-dihexaoyl-*sn*-glycero-3-phosphocholine; [PC], total lipid concentration; MD, molecular dynamics; APL, area per lipid; DEPT, distortionless enhancement by polarization transfer; HSQC, hetero-nuclear single quantum coherence; TOCSY, total correlation spectroscopy

Table 1: Resonance assignments used for spectra and relaxation rate analyses along with their labels.

Label	Nucleus	Assignment	Chemical shift range (ppm)
Δ_1	^{1}H	DMPC *sn*-1/2 CH_3	(0.82 ~ 0.76)* to 0.7
Δ_2	^{1}H	DHPC *sn*-1/2 CH_3	0.9 to (0.82 ~ 0.76)*
Δ_3	^{13}C	DMPC *sn*-1/2 C_4-C_{11}	30.9 to 29
Δ_4	^{13}C	DMPC *sn*-1/2 C_{12}	32.7 to 31.8
Δ_5	^{13}C	DMPC *sn*-1/2 C_{13}	23.1 to 22.5
Δ_6	^{1}H	PC *sn*-3 N($C\underline{H}_3$)$_3$	3.2 to 3.1
Δ_7	^{13}C	PC *sn*-3 N($\underline{C}H_3$)$_3$	54.1 to 53.7

*Because the methyl resonances shift with the *q* ratio, the upper (lower) limit of the integration ranges for signals from DMPC (DHPC) was determined at the position of the lowest intensity between the separated signals.

Table 2: R_2 relaxation rate constants of ^{1}H resonances in bicelles with different *q* ratios.

q	Δ_1 R_2 (s^{-1})	Δ_6 R_2 (s^{-1})
0.5	3.68 ± 0.21	2.12 ± 0.02
1.0	7.94 ± 0.11	2.46 ± 0.05

Table 3: R_1 relaxation rate constants of ^{13}C resonances in bicelles with different *q* ratios.

q	Δ_3 R_1 (s^{-1})	Δ_4 R_1 (s^{-1})	Δ_5 R_1 (s^{-1})	Δ_7 R_1 (s^{-1})
0.5	1.27 ± 0.03	0.61 ± 0.10	0.52 ± 0.06	1.43 ± 0.03
1.0	1.32 ± 0.04	0.60 ± 0.07	0.61 ± 0.05	1.62 ± 0.02

Figures

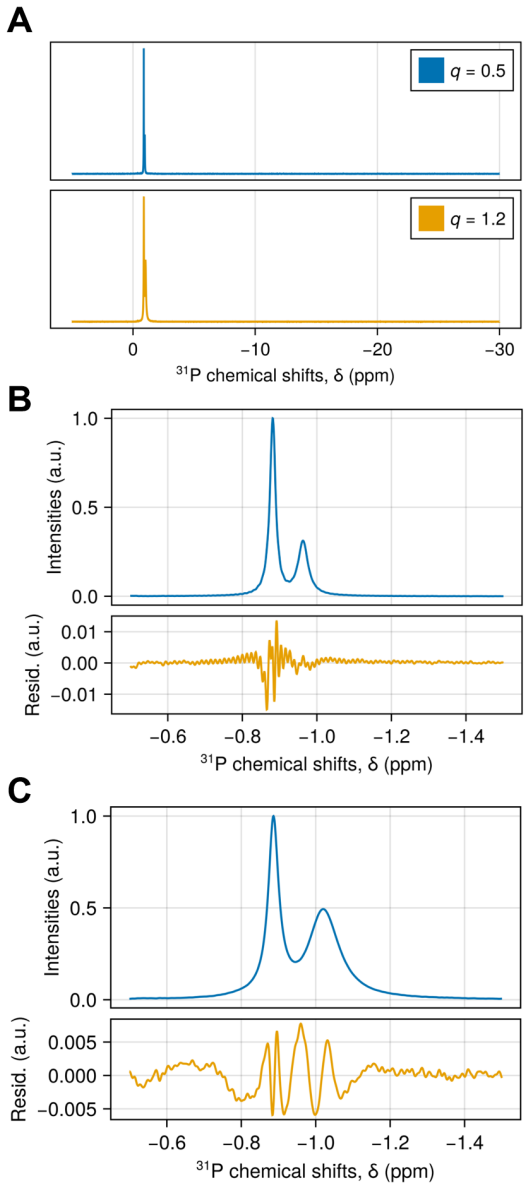

Figure 1: ^{1}H-decoupled ^{31}P NMR spectra of bicelles with different *q* ratios.

The *q* values were estimated using ^{1}H NMR spectra (Eq. 1). Each measurement was conducted at 25°C. The total phospholipid concentrations [PC] were maintained at 100 mM the for $q = 0.5$ and $q = 1.2$ bicelles. (A) ^{1}H-decoupled ^{31}P NMR spectra of bicelle solutions between 5 and -30 ppm with the indicated *q* values. (B and C) ^{1}H decoupled ^{31}P NMR spectra of bicelle solutions with q=0.5 (B) and q=1.2 (C) in the region containing phospholipid signals. The bottom figures in B and C display the residuals after fitting the spectra as sums of two-Lorentzian distributions for the $q = 0.5$ and $q = 1.2$ samples, respectively.

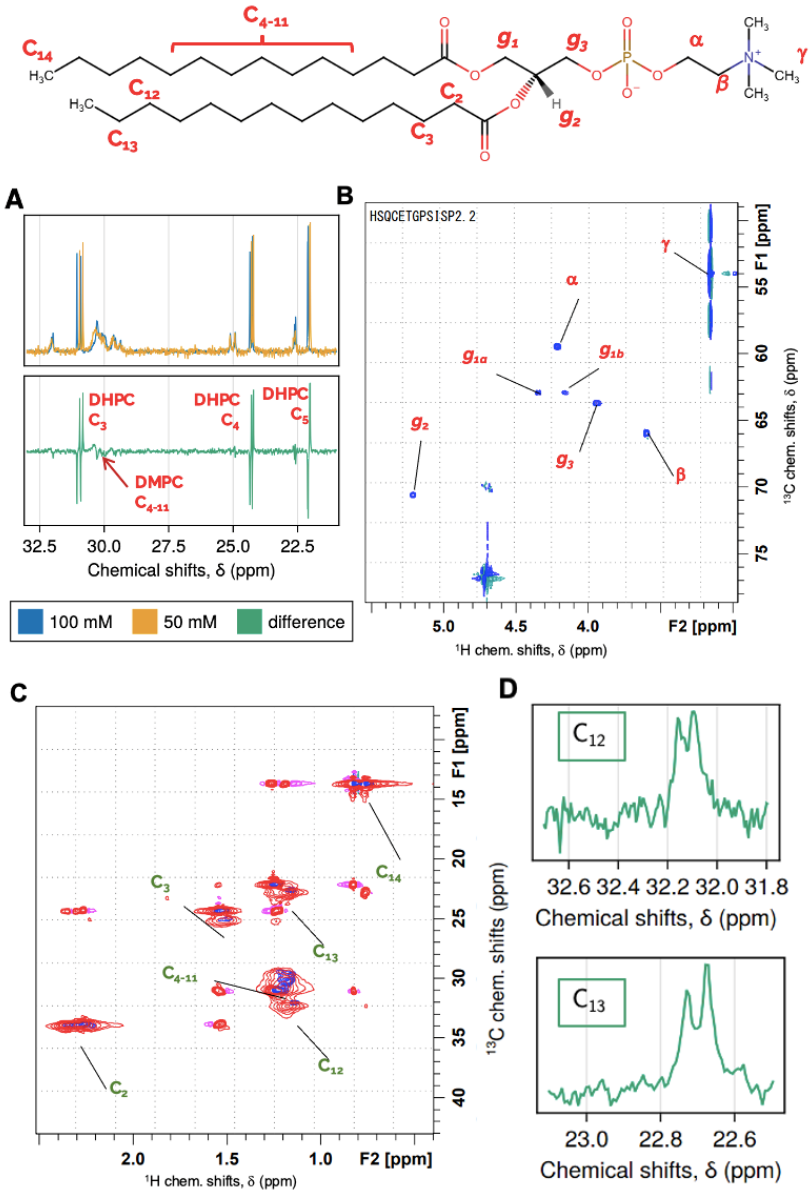

Figure 2: Reference spectra for resonance and lipid phase assignments in isotropic bicelles. (Top) Chemical structure of DMPC, including the assignments of various nuclei (positions) along its length. (A) A section of the acyl chain region of DEPT-45 spectra for bicelles with q = 0.5 and [PC] = 100 mM or 50 mM as indicated. The difference (50 mM – 100 mM) spectrum is included to emphasize the upfield shift of the sharp DHPC $C_{3\text{-}5}$ resonances upon bicelle dilution. Also labeled in the difference spectrum is the downfield shift of the central DMPC $C_{4\text{-}11}$ chain. (B) Headgroup region of ^{1}H–^{13}C HSQC spectra, where ^{13}C resonance assignments are based on their correlations with ^{1}H resonances [21]. (C) Acyl chain region of ^{1}H–^{13}C HSQC (blue) and HSQC-TOCSY (red) spectra. Sequential ^{13}C assignments were performed by assuming that nuclei connected through fewer bonds produce more intense cross-peaks than those connected through more bonds. (D) DMPC acyl chain C_{12} and C_{13} regions of DEPT-45 spectra show apparent splitting of respective resonances despite a low signal-to-noise ratio.

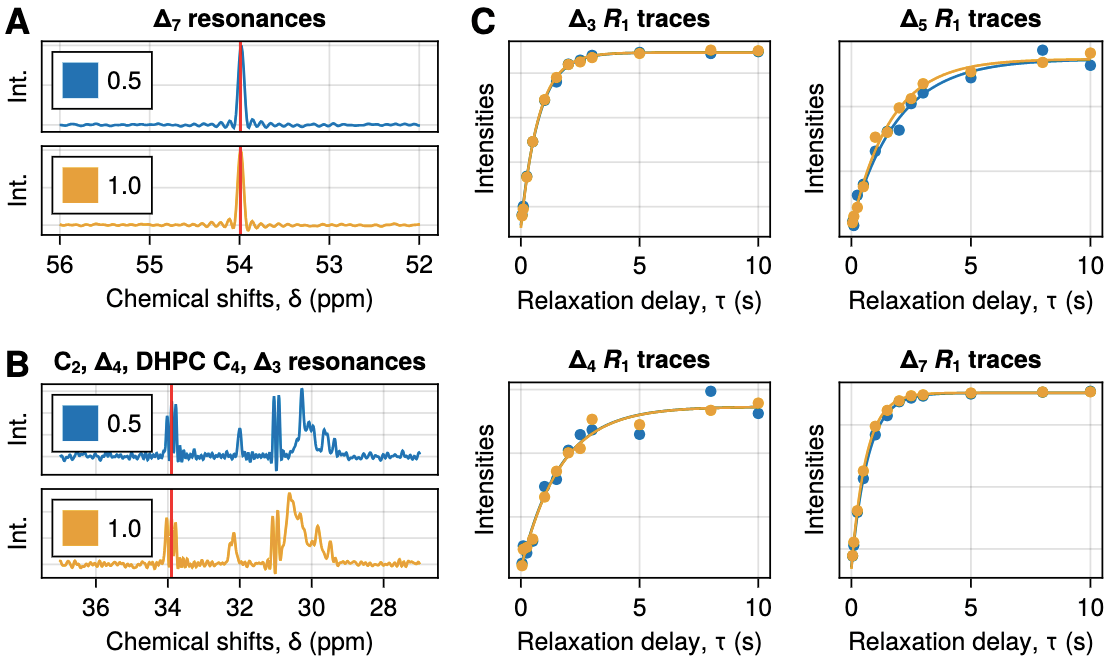

Figure 3: ^{13}C NMR spectra for bicelles with $q = 0.5$ and $q = 1$ and decays for ^{13}C R_1 relaxation. (A) Headgroup γ peaks for bicelles from the R_1 spectra with 10-s relaxation time. The red line serves as a guide for the chemical shifts indicating no perturbations in the structure of the choline methyl groups. (B) Acyl chain resonances for the bicelles from the R_1 spectra with 10-s relaxation time. The red line serves as a guide for the chemical shifts indicating no perturbations in the structure of C_2 carbons. (C) Traces of integrated intensities from the R_1 experiments along with fitted recovery curves. Plotted intensities and curves were scaled to have matching A_1 parameters in Eq. 4.

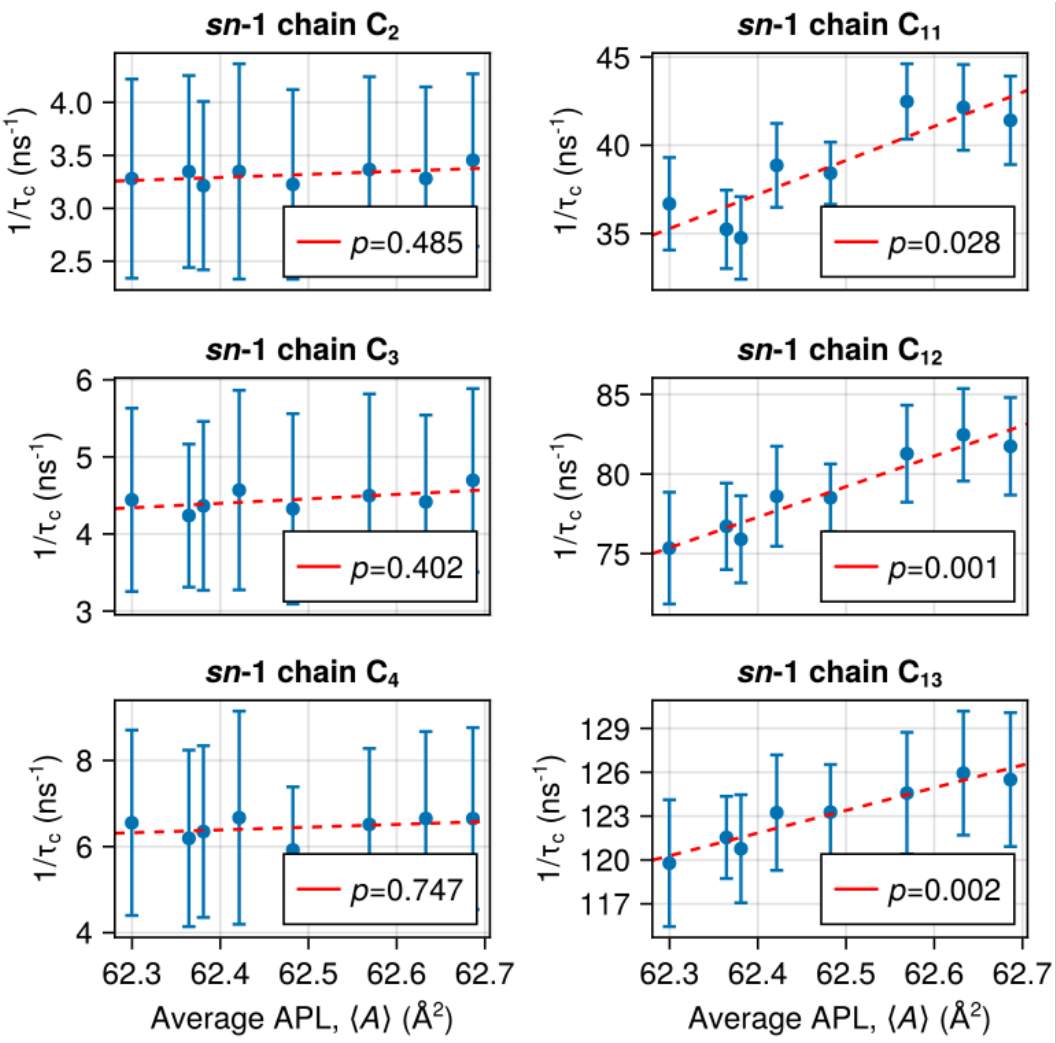

Figure 4: Decay rates of time correlation functions of H–C bond angle in acyl chains of pure DMPC lipids with varying APLs. The dashed lines are the best-fit lines, and *p* values for the *F*-test of overall significance are indicated in the respective subplots. Error bars indicate standard deviations of the correlation rates over the lipids in the simulation box ($N = 128$).

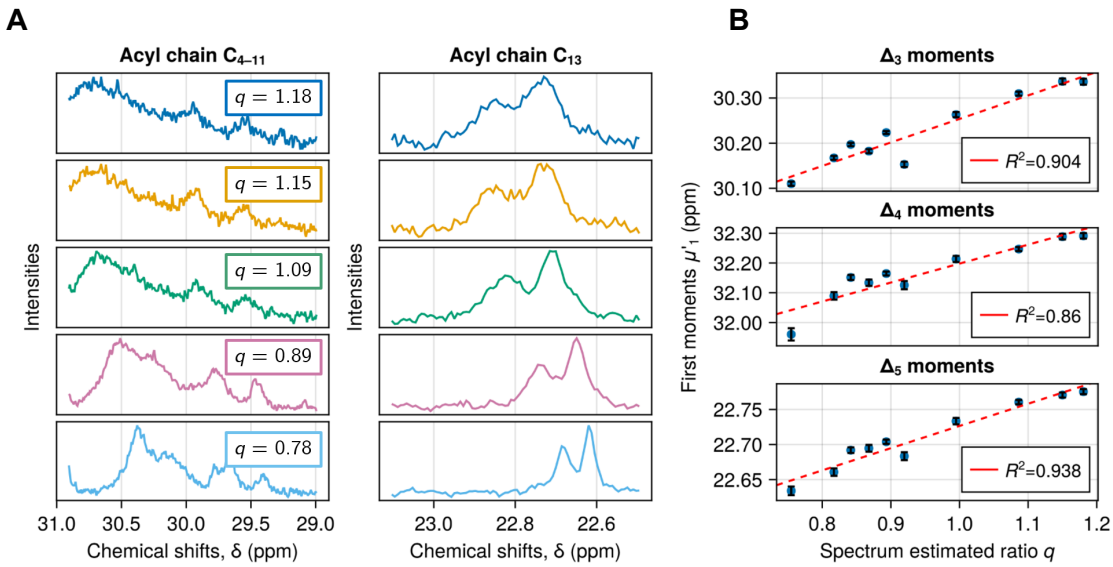

Figure 5: DEPT-45 spectra of bicelles with different *q* ratio and dependence of ^{13}C chemical shifts of acyl carbons on *q* ratio (A) (left) Representative NMR signals from DMPC acyl chain C_4-C_{11}. (right) Representative NMR signals from DMPC acyl chain C_{13} (B) First moments of respective resonances against the *q* ratios estimated using ^{1}H spectra. Included are R^2 values from simple linear regression (dashed line).

CRediT authorship contribution statement

Bon Leif Dominguez Amalla: Conceptualization, Data curation, Writing – original draft, Investigation, Methodology. **Hiroyuki Kumeta:** Data curation, Methodology, Writing – review & editing. **Satoshi Nagao:** Methodology, Writing – review & editing. **Koichiro Ishimori:** Project administration, Conceptualization, Writing – review & editing, Investigation, Supervision.

Declaration of competing interest

The authors declared no potential conflicts of interest with respect to the research, authorship, and publication of this article.

Acknowledgements

This research was supported by JSPS KAKENHI Grant Number JP19H05769 (K.I.). We thank Dr. Takeshi Uchida of Hokkaido University for his invaluable advice on experimental procedures and for the productive discussions.

References

[1] D. Marsh, Handbook of Lipid Bilayers, 2nd Edition ed., CRC Press, Boca Raton, 2013.

[2] Z. Cournia, T.W. Allen, I. Andricioaei, B. Antonny, D. Baum, G. Brannigan, N.-V. Buchete, J.T. Deckman, L. Delemotte, C. del Val, R. Friedman, P. Gkeka, H.-C. Hege, J. Hénin, M.A. Kasimova, A. Kolocouris, M.L. Klein, S. Khalid, M.J. Lemieux, N. Lindow, M. Roy, J. Selent, M. Tarek, F. Tofoleanu, S. Vanni, S. Urban, D.J. Wales, J.C. Smith, A.-N. Bondar, Membrane Protein Structure, Function, and Dynamics: a Perspective from Experiments and Theory, J. Membrane Biol. 248 (2015) 611-640. 10.1007/s00232-015-9802-0.

[3] M.F. Brown, Soft Matter in Lipid–Protein Interactions, Annu. Rev. Biophys. 46 (2017) 379-410. 10.1146/annurev-biophys-070816-033843.

[4] V. Corradi, E. Mendez-Villuendas, H.I. Ingólfsson, R.-X. Gu, I. Siuda, M.N. Melo, A. Moussatova, L.J. DeGagné, B.I. Sejdiu, G. Singh, T.A. Wassenaar, K. Delgado Magnero, S.J. Marrink, D.P. Tieleman, Lipid–Protein Interactions Are Unique Fingerprints for Membrane Proteins, ACS Cent. Sci. 4 (2018) 709-717. 10.1021/acscentsci.8b00143.

[5] A.G. Lee, Lipid–protein interactions in biological membranes: a structural perspective, Biochim. Biophys. Acta 1612 (2003) 1-40. 10.1016/S0005-2736(03)00056-7.

[6] L. Frey, N.-A. Lakomek, R. Riek, S. Bibow, Micelles, Bicelles, and Nanodiscs: Comparing the Impact of Membrane Mimetics on Membrane Protein Backbone Dynamics, Angewandte Chemie International Edition 56 (2017) 380-383. 10.1002/anie.201608246.

[7] K. Klöpfer, F. Hagn, Beyond detergent micelles: The advantages and applications of non-micellar and lipid-based membrane mimetics for solution-state NMR, Prog. Nuc. Mag. Res. Spec. 114-115 (2019) 271-283. 10.1016/j.pnmrs.2019.08.001.

[8] E.J. Dufourc, Bicelles and nanodiscs for biophysical chemistry, Biochim. Biophys. Acta 1863 (2021) 183478. 10.1016/j.bbamem.2020.183478.

[9] S. Majeed, A.B. Ahmad, U. Sehar, E.R. Georgieva, Lipid Membrane Mimetics in Functional and Structural Studies of Integral Membrane Proteins, Membranes 11 (2021) 685.

[10] U.H.N. Dürr, M. Gildenberg, A. Ramamoorthy, The Magic of Bicelles Lights Up Membrane Protein Structure, Chem. Rev. 112 (2012) 6054-6074. 10.1021/cr300061w.

[11] A. Andersson, L. Mäler, Magnetic Resonance Investigations of Lipid Motion in Isotropic Bicelles, Langmuir 21 (2005) 7702-7709. 10.1021/la0513003.

[12] E.F. Kot, A.S. Arseniev, K.S. Mineev, Behavior of Most Widely Spread Lipids in Isotropic Bicelles, Langmuir 34 (2018) 8302-8313. 10.1021/acs.langmuir.8b01454.

[13] E.F. Kot, S.A. Goncharuk, A.S. Arseniev, K.S. Mineev, Phase Transitions in Small Isotropic Bicelles, Langmuir 34 (2018) 3426-3437. 10.1021/acs.langmuir.7b03610.

[14] M.N. Triba, D.E. Warschawski, P.F. Devaux, Reinvestigation by Phosphorus NMR of Lipid Distribution in Bicelles, Biophys. J. 88 (2005) 1887-1901. https://doi.org/10.1529/biophysj.104.055061.

[15] M.J. Abraham, T. Murtola, R. Schulz, S. Páll, J.C. Smith, B. Hess, E. Lindahl, GROMACS: High performance molecular simulations through multi-level parallelism from laptops to supercomputers, SoftwareX 1-2 (2015) 19-25. 10.1016/j.softx.2015.06.001.

[16] F. Grote, A.P. Lyubartsev, Optimization of Slipids Force Field Parameters Describing Headgroups of Phospholipids, J. Phys. Chem. B 124 (2020) 8784-8793. 10.1021/acs.jpcb.0c06386.

[17] J.P.M. Jämbeck, A.P. Lyubartsev, Derivation and Systematic Validation of a Refined All-Atom Force Field for Phosphatidylcholine Lipids, J. Phys. Chem. B 116 (2012) 3164-3179. 10.1021/jp212503e.

[18] K.J. Glover, J.A. Whiles, G. Wu, N.-j. Yu, R. Deems, J.O. Struppe, R.E. Stark, E.A. Komives, R.R. Vold, Structural Evaluation of Phospholipid Bicelles for Solution-State Studies of Membrane-Associated Biomolecules, Biophys. J. 81 (2001) 2163-2171. 10.1016/S0006-3495(01)75864-X.

[19] A. Andersson, L. Mäler, Size and Shape of Fast-tumbling Bicelles as Determined by Translational Diffusion, Langmuir 22 (2006) 2447-2449. 10.1021/la053177l.

[20] R.N. Purusottam, L. Sénicourt, J.-J. Lacapère, P. Tekely, Probing the gel to liquid-crystalline phase transition and relevant conformation changes in liposomes by 13C magic-angle spinning NMR spectroscopy, Biochim. Biophys. Acta 1848 (2015) 3134-3139. 10.1016/j.bbamem.2015.09.011.

[21] P.A. Luchette, T.N. Vetman, R.S. Prosser, R.E.W. Hancock, M.-P. Nieh, C.J. Glinka, S. Krueger, J. Katsaras, Morphology of fast-tumbling bicelles: a small angle neutron scattering and NMR study, Biochim. Biophys. Acta 1513 (2001) 83-94. 10.1016/S0005-2736(01)00358-3.

[22] J. Lind, J. Nordin, L. Mäler, Lipid dynamics in fast-tumbling bicelles with varying bilayer thickness: Effect of model transmembrane peptides, Biochim. Biophys. Acta 1778 (2008) 2526-2534. 10.1016/j.bbamem.2008.07.010.

[23] M.L. Greenfield, L.M. Martin, F. Joodaki, Computing Individual Area per Head Group Reveals Lipid Bilayer Dynamics, J. Phys. Chem. B 126 (2022) 10697-10711. 10.1021/acs.jpcb.2c04633.

[24] J.F. Nagle, S. Tristram-Nagle, Structure of lipid bilayers, Biochim. Biophys. Acta 1469 (2000) 159-195. 10.1016/S0304-4157(00)00016-2.

[25] M. Vestergaard, J.F. Kraft, T. Vosegaard, L. Thøgersen, B. Schiøtt, Bicelles and Other Membrane Mimics: Comparison of Structure, Properties, and Dynamics from MD Simulations, J. Phys. Chem. B 119 (2015) 15831-15843. 10.1021/acs.jpcb.5b08463.

[26] H. Akutsu, Structure and dynamics of phospholipids in membranes elucidated by combined use of NMR and vibrational spectroscopies, Biochim. Biophys. Acta 1862 (2020) 183352. 10.1016/j.bbamem.2020.183352.

[27] E. Morvan, N. Taib-Maamar, A. Grélard, A. Loquet, E.J. Dufourc, Bio-membranes: Picosecond to second dynamics and plasticity as deciphered by solid state NMR, Biochim. Biophys. Acta 1865 (2023) 184097. 10.1016/j.bbamem.2022.184097.

[28] R.R. Vold, R.S. Prosser, Magnetically Oriented Phospholipid Bilayered Micelles for Structural Studies of Polypeptides. Does the Ideal Bicelle Exist?, J. Mag. Res. B 113 (1996) 267-271. 10.1006/jmrb.1996.0187.